Ranjana, M.; Kashyap, Namita N.; Mitra, Prajoy Kumar; Sunil, Dhanya; Sudhakar, Y. N.; Vennapusa, Sivaranjana Reddy; Raju, Ramesh; Tittonen, Ilkka; Upadhya, Dinesh

# Chemical synthesis and analytical profiling of NTSH : a versatile probe for hydrogen sulfide sensing and cellular imaging

*Published in:*
Materials Research Express

*DOI:*
10.1088/2053-1591/ad94d3

Published: 27/11/2024

*Document Version*
Publisher's PDF, also known as Version of record

Materials Research Express



**PAPER** • **OPEN ACCESS**

# Chemical synthesis and analytical profiling of NTSH: a versatile probe for hydrogen sulfide sensing and cellular imaging

To cite this article: Ranjana M *et al* 2024 *Mater. Res. Express* **11** 115101

Materials Research Express

PAPER

# Chemical synthesis and analytical profiling of NTSH: a versatile probe for hydrogen sulfide sensing and cellular imaging

**Ranjana M**[1], **Namita N Kashyap**[2], **Prajoy Kumar Mitra**[3], **Dhanya Sunil**[1,*], **Sudhakar Y N**[1], **Sivaranjana Reddy Vennapusa**[3], **Ramesh Raju**[4], **Ilkka Tittonen**[4] **and Dinesh Upadhya**[2]

[1] Department of Chemistry, Manipal Institute of Technology, Manipal Academy of Higher Education, Manipal-576104, Karnataka, India
[2] Centre for Molecular Neurosciences, Kasturba Medical College, Manipal Academy of Higher Education, Manipal-576104, Karnataka, India
[3] School of Chemistry, Indian Institute of Science Education and Research, Thiruvananthapuram-695016, Kerala, India
[4] Department of Electronics and Nanoengineering, Aalto University, PO Box 13500, FI-00076, Finland
[*] Author to whom any correspondence should be addressed.

**E-mail:** dhanyadss3@gmail.com **and** dhanya.s@manipal.edu

**Keywords:** $H_2S$ sensor, electrochemical sensing, colorimetric sensing, fluorometric sensing, cellular imaging, endogenous $H_2S$

Supplementary material for this article is available online

**OPEN ACCESS**

**RECEIVED**
11 August 2024

**REVISED**
28 October 2024

**ACCEPTED FOR PUBLICATION**
19 November 2024

**PUBLISHED**
27 November 2024



## Abstract

The development of novel probes featuring diverse structural motifs, with promising applications in $H_2S$ detection and cellular imaging remains a central focus of scientific research. This study details the synthesis of 4-methyl-N-(6-nitro-1,3-dioxo-1*H*-benzo[*de*]isoquinolin-2(3*H*)-yl)benzenesulfonamide (NTSH), which involves a condensation reaction between commercially available 4-nitro-1,8-naphthalic anhydride and *p*-toluenesulfonyl hydrazide in glacial acetic acid. The $H_2S$ probe exhibits detection limits of 166 μM in fluorometric, 15.08 mM in absorbance, 2.48 mM in colorimetric, and 29 nM in electrochemical studies. The versatility of NTSH in sensing endogenous $H_2S$ and bioimaging of HEK 293T cells highlights its potential applicability in chemical biology research. The tendency of NTSH to undergo chemical changes in the presence of $H_2S$ to induce noticeable optical and electrochemical responses could lay the groundwork for creating sensitive and selective sensing platforms.

## 1. Introduction

In the mammalian system, the majority of endogenous $H_2S$ production occurs through enzymatic reactions involving cystathionine $\beta$-synthase, cystathionine $\gamma$-lyase, and 3-mercapto pyruvate sulfurtransferase [1–3]. Sensing $H_2S$ is crucial in biological systems because the small molecule operates as a double-edged sword in several disease processes. The gas exhibits a toxicity profile analogous to that of carbon monoxide (CO), as it binds to iron within the mitochondrial cytochrome enzymes, thereby obstructing cellular respiration. The bell-shaped dose–response curves for $H_2S$ are well acknowledged and tested, which refers to a pattern where the biological effect of $H_2S$ follows a non-linear relationship with its concentration [4]. At lower concentrations, $H_2S$ may have beneficial effects, such as serving as a signaling molecule or gasotransmitter in various physiological processes. However, at higher concentrations, it can become toxic, leading to adverse effects on cellular function and tissue integrity, which proves the immense importance of $H_2S$ sensing [5, 6]. In contrast, high concentrations of $H_2S$ have a strong anticancer effect by inhibiting signaling pathways linked to metastasis and proliferation, regulating glycolysis, and arresting the cell cycle [7, 8]. Under pathological concentration, $H_2S$ accelerates the cell cycle, promotes angiogenesis, inhibits apoptosis, and ultimately results in neoplasia in tumors. Therefore, accurate measurement of $H_2S$ sheds light on the physiological roles of $H_2S$ in complex tissues and mammalian organs.

Numerous approaches for detecting $H_2S$, including methylene blue, ion-selective electrodes, and gas chromatography (GC) methods, have been developed [9, 10]. However, these methods possess certain

drawbacks. For instance, the methylene blue method exhibits low detection sensitivity in the micromolar range. Additionally, estimating the concentration of $H_2S$ may be inaccurate due to sulfides escaping from acid-labile stores and the volatility of $H_2S$. Attention must be paid to the long equilibration time in the $H_2S$ ion-selective electrodes method, whereas the airtightness of equipment is crucial in the GC method [11, 12]. Colorimetric and fluorescent probes are considered efficient tools to achieve more sensitive and convenient detection of $H_2S$ in complex biological systems. They offer advantages such as low cost, high biocompatibility, real-time sensing, and high selectivity. Consequently, optical probes for sensitive $H_2S$ detection, both *in vitro* and *in vivo*, have become a focal point in analytical research. Several optical probes for $H_2S$ detection, both colorimetric and fluorometric have been designed based on different sensing mechanisms and synthesized for the selective recognition and quantitative analysis of $H_2S$, particularly in living cells and tissues. Compared to other $H_2S$ detection methods, fluorescent probes offer high sensitivity and excellent cell membrane penetration capability. Yang *et al* synthesized a fluorescent probe using a coumarin derivative for *in situ* detection and imaging of $H_2S$. The probe effectively penetrated cell membranes, localizing in the cytoplasm, nucleus, lysosomes, and mitochondria to detect $H_2S$ [13]. Given the high quantum yield and mitochondrial targeting abilities, rhodamine-based fluorescent probes were also reported [14]. Other fluorescent probes used in detecting $H_2S$ in biological systems include molecular systems based on BODIPY [15], chromone and flavone [16], naphthalene [17], phenanthroimidazole [18] etc.

In fluorescence imaging methods, autofluorescence poses a serious problem since it can mask or obstruct the identification of fluorescent signals. When stimulated by a particular wavelength, the inherent light emission from biological tissues or other components inside a sample can obscure the signals obtained from fluorescent probes that are specifically targeted. Autofluorescence from intrinsic biomolecules in tissues like the kidney and liver poses a significant challenge for imaging in depth. Therefore, it is imperative to decrease autofluorescence for several reasons, including reduced background noise, increased clarity of images, and improved image depth, which are affected by scattering and absorption of light. The development of red-emitting, water-soluble, two-photon absorbing dyes is highlighted as a solution to minimize autofluorescence [19]. Moreover, fluorophores with longer emission wavelengths are advantageous and are highly sought after in fluorescence imaging due to their ability to reduce autofluorescence, enhance image contrast, penetrate deeper into tissues, and minimize photodamage. This makes them valuable tools for achieving high-quality, accurate imaging in various biological research applications.

Naphthalimide is acknowledged as a classical fluorescent platform with exceptional two-photon properties. The electron-withdrawing nitro group present in the naphthalimide framework creates an 'A-$\pi$-A' electronic structure that could result in a weak fluorescent emission signal. In biological systems, reducing the nitro group upon exposure to gasotransmitters, including CO and $H_2S$, could aid its transformation into an amine moiety with a strong electron-donating nature, generating a 'D-$\pi$-A' electronic structure. This structural change could induce a robust optical or electrochemical signal. As a typical donor-$\pi$-acceptor (D-$\pi$-A) fluorescent dye with suitable substituents appended to the structural unit, 1,8-naphthalimide has stable optical properties and high fluorescence quantum yield. Moreover, nitronaphthalimide-based fluorescent probes with less autofluorescence features for biological imaging and endogenous $H_2S$ detection have not been reported in detail.

The literature survey illustrates reports on naphthalimide-based CO sensors, wherein a nitro group is located at the 3-position of the polycyclic unit. Zhang *et al* reported a turn-on fluorescent probe featuring a 3-nitronapthalimide framework linked to an endoplasmic reticulum (ER) targeting sulfonamide segment for CO detection [20]. This biocompatible probe could monitor exogenous and endogenous CO level changes in the ER with a high signal-to-noise ratio, fast recognition speed, high selectivity, sensitivity, and photostability. To enable targeted detection of lysosomal CO in living cells, Dhara *et al* developed a morpholine-based nitronaphthalimide probe [21], which could selectively sense CO in an aqueous buffer at pH 7.4 upon reduction of the nitro group to a highly fluorescent amino unit. Later, Sarkar *et al* designed a morpholine-based fluorescent probe that localizes in the nucleus for selective intracellular CO sensing in an aqueous buffer at pH 7.4 at 37 °C [22]. However, significant cytotoxicity was observed after 4 h of incubation at concentrations exceeding 7 μM. Montoya and coworkers developed two fluorescent turn-on sensors featuring a nitro group at the 4-position, which demonstrated high selectivity for $H_2S$ in living cells over other thiol analytes and reactive nitrogen, sulfur, and oxygen species [23]. Moreover, the literature survey indicates that sulfonylurea compounds, which are known inhibitors of ATP-sensitive $K^+$ channels, exhibit selective binding to the proteins. Consequently, fluorescent analogs of sulfonylurea are commonly employed to label the cellular organelle. Tang *et al* synthesized a fluorophore by reacting sulphonyl chloride with ethylene diamine to sense formaldehyde [24]. Later, they combined the same targeting moiety and an azide unit for $H_2S$ detection through reduction reaction-induced fluorescence responses [25]. In 2018, Xu *et al* used the same sulphonyl chloride derivative with nitro naphthalic anhydride to sense cellular nitro reductase in hypoxia conditions [26]. Angela Bamesberger *et al* reported a 'turn-on' fluorescent probe with significant 30-fold fluorescence enhancement in the presence of $H_2S$ [27]. To the best of our knowledge, substituted 4-nitro naphthalimide based probes have not been studied as $H_2S$ sensors

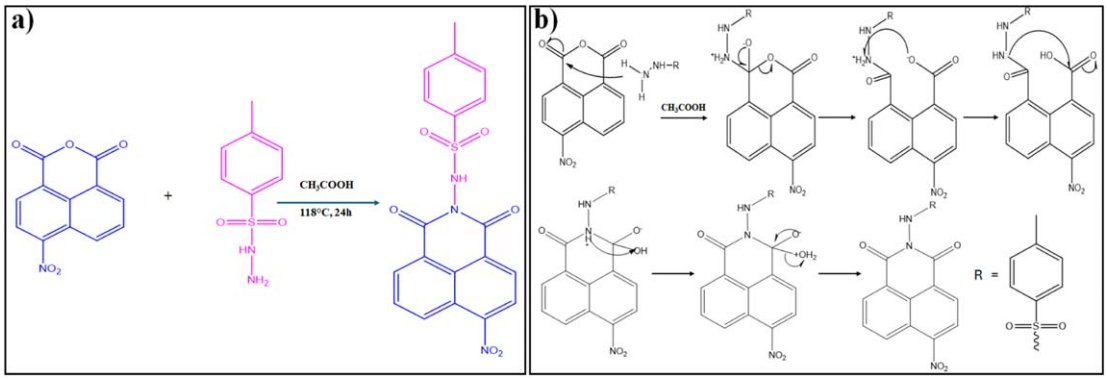


**Scheme 1.** (a) Synthetic route for NTSH. (b) Plausible mechanism of acetic acid catalyzed imidation reaction.

through electrochemical methods till now. This highlights a significant gap in the existing literature, as the electrochemical approach can offer distinct advantages, such as enhanced sensitivity and the ability to detect lower concentrations of analytes in real-time.

As there are only a few studies reported on nitro naphthalimides as $H_2S$ sensors, we were motivated to design an $H_2S$-detecting naphthalimide framework appended with a nitro group as the $H_2S$ identification site with good selectivity over CO. The present study is thus focused on constructing a new toluene sulphonyl hydrazide attached nitro napthalimide, 4-methyl-N-(6-nitro-1,3-dioxo-1*H*-benzo[*de*]isoquinolin-2(3*H*)-yl) benzenesulfonamide (NTSH) as an $H_2S$ sensor based on initial theoretical Density Functional theory (DFT) simulations [28]. Further, the effectiveness of the synthesized probe in detecting $H_2S$ through electrochemical, absorbance, colorimetric, and fluorometric methods is demonstrated. Furthermore, the possible applications of NTSH in cell imaging and detecting endogenous $H_2S$ are also explored.

## 2. Materials and methods

4-Nitro-1,8-naphthalic anhydride, *p*-Toluene sulphonyl hydrazide, Sodium sulfide ($H_2S$ releasing agent), Di-Sodium hydrogen phosphate, Potassium phosphate monobasic, and Sodium chloride, were procured from Sigma Aldrich and were used as such. Ethanol, Acetone, Dimethyl sulfoxide (DMSO), Hexane, and Ethyl acetate were procured from SRL chemicals. All chemicals used were of analytical grade. Milli-Q water was used to prepare the phosphate buffer (PBS of pH 7.4).

### 2.1. Synthesis of 4-methyl-*N*-(6-nitro-1,3-dioxo-1*H*-benzo[*de*]isoquinolin-2(3*H*)yl) benzenesulfonamide (NTSH)

4-nitro-1,8-naphthalic anhydride (60 mg, 0.2467 mmol) and *p*-toluene sulphonyl hydrazide (55.14 mg, 0.2960 mmol) were added in glacial acetic acid (10 ml). The reaction mixture was refluxed for 24 h under stirring at 340 rpm and allowed to cool down to room temperature (scheme 1(a)). About 10% (w/v) sodium bicarbonate solution was added to the reaction mixture to achieve complete neutralization. The precipitate formed was filtered, washed with distilled water, and dried at room temperature for 48 h to obtain NTSH.

### 2.2. Chemical characterisation of NTSH

$^1H$ and $^{13}C$ NMR spectra were recorded in Bruker Ascend 400 MHz, spectrophotometer. $^1H$ NMR spectrum was obtained with 16 scans, while the $^{13}C$ NMR spectrum was recorded with 1024 scans. About 5 mg and 10 mg of NTSH solid was dissolved in 0.4 ml $CDCl_3$ for recording $^1H$ and $^{13}C$ NMR, respectively. The IR spectrum of solid NTSH was recorded using IRSpirit-X FTIR Spectrometer (Shimadzu, Japan). The mass spectrum of NTSH was recorded using a Gas Chromatography-Mass spectrometer (GC -2010, Shimadzu, Japan), and that of reduced NTSH was recorded in MALDI-TOF mass spectrometer (Ultraflextreme, Bruker) that operates in both linear and reflectron ionization modes.

### 2.3. Theoretical studies

Theoretical calculations were conducted in the gas phase utilizing Gaussian 16 software. The ground-state geometries of NTSH were optimized without symmetry constraints, employing the hybrid density functional B3LYP in conjunction with the 6–31+G(d) basis set. The binding energies between the gasotransmitters (CO and $H_2S$) and the nitro group of NTSH were computed using the following equation;

Binding energy = $E_{Complex}-(E_{Binder}+E_{CO/H2S})$, where $E_{Complex}$, $E_{Binder}$, and $E_{CO/H2S}$ are the energies of the bound complex, the various binders, and $CO/H_2S$, respectively.

### 2.4. Electrochemical studies

Cyclic voltammetry (CV) was performed using the Zahner Zennium Pro workstation, and square wave voltammetry (SWV) was conducted using Biologic SP50-e. CV of neat NTSH was recorded in different scan rates from 1–100 mV $s^{-1}$. *In situ* studies were performed at 5 mV $s^{-1}$. The system was also studied at 10 and 100 mV $s^{-1}$. A three-electrode setup was utilized for voltammetric investigations, comprising platinum wire as the counter electrode and a silver/silver chloride (Ag/AgCl/KCl (sat.)) electrode as the reference electrode. The working electrode was stainless-steel with 1 cm × 1 cm dimensions. Electrolyte solution containing 0.82 mg of NTSH in 20 ml of DMSO-PBS (1:50) was prepared. $Na_2S$ in distilled water with concentrations ranging from 0.05 to 8.3 mM were successively added into the electrolyte to record cyclic and square wave voltammograms. To find the limit of detection (LOD), square wave voltammetry (SWV) was conducted using varying $Na_2S$ concentrations (0.5–63.5 nM) at 10 Hz, with a pulse amplitude of 25 mV, a step potential of 0.5 V, and a scan rate of 100 mV $s^{-1}$. All measurements were conducted at ambient temperature (23 ± 3 °C). A minimum of three replicates were performed for each test. The x-ray Photoelectron Spectroscopy (XPS) spectra were recorded using an Omicron Nanotechnology Ltd XPS device with Al -K$\alpha$ (h$\nu$ = 1486.7 eV) in the scan range of 236.7 to 1486.7 eV.

### 2.5. Optical studies

To perform absorbance, emission, and colorimetric measurements, NTSH was dissolved in DMSO and PBS to prepare stock solutions of 1000 μM, which were further diluted using 1:6 DMSO:PBS at room temperature (r.t.) to achieve a final probe concentration of 100 μM. A stock solution of 0.1 M $Na_2S$ was prepared using distilled water. $Na_2S$ concentration was raised in succession from 0.32 to 30.2 mM for further experiments. For selectivity studies of NTSH, fluorescence emission measurements were recorded at an excitation wavelength of 430 nm. Stock solutions of $Na_2S$ (0.1 mM), and biothiols like Glutathione and Cysteine (GSH and Cys: 0.2 mM each) were used.

Absorbance measurements were carried out using a Shimadzu UV-visible spectrophotometer 2201 with a bandwidth of 3.0 nm and a wavelength range of 200–800 nm at a medium scan speed. Fluorescence measurements were conducted at an excitation wavelength of 430 nm using a JASCO FP 8300 spectrofluorometer and a Horiba Fluorolog spectrofluorometer equipped with a Xenon lamp as the light source. The scan wavelength range was set from 440 nm to 800 nm, with slit bandwidths of 2.5 nm for both excitation and emission. A response time of 10 msec and a scanning speed of 1000 nm $sec^{-1}$ were used for the measurements. Time-correlated single photon counting (TCSPC) measurements were carried out in Horiba Datastation V2.5, Nano-LED-440L, with a pulse duration of < 100 ps. Colorimetric studies were conducted using a Systronics photoelectric colorimeter in absorbance mode, equipped with a 430 nm filter.

### 2.6. Biological studies

Human embryonic kidney cells (HEK 293T) were cultured in Dulbecco's Modified Eagle Medium (DMEM) (Thermofisher 11965092) supplemented with 10% fetal bovine serum (RM9955-himedia) and incubated at 37 °C in 5% $CO_2$ for 24 h to perform biological studies. To assess the cytotoxicity of NTSH, cells were seeded into 96-well dishes at a density of $10^4$ cells per well and incubated overnight. These cells were then treated with varying concentrations of NTSH (5–30 μM) and incubated for 48 h. Further, the medium was removed, and the cells were treated with 3-(4,5-dimethylthiazol-2-yl)-2,5-diphenyltetrazolium bromide (MTT) solution with a final concentration of 0.5 mg $mL^{-1}$, after which the plates were returned to the incubator for 4 h. The supernatant was carefully removed and 200 μl DMSO was added to each well. Absorbance was measured using a BioTek Synergy H1 microplate reader at 570 nm. The percentage cell viability was calculated using the following formula;

Percentage cell viability = ODsample/ODcontrol × 100, where $OD_{sample}$ and $OD_{control}$ represent the optical density of the sample and control, respectively.

To perform bioimaging using NTSH, coverslips were placed in a 24-well plate and coated with Poly-D Lysine overnight. About $5 \times 10^4$ cells were seeded into each well and incubated for 24 h at 37 °C in 5% $CO_2$. Further, 5 μM of NTSH was added into wells and incubated for 30 min, followed by 500 μM $Na_2S$ and incubated for another 30 min. To maintain accuracy and avoid bias, a control well with no treatment, a well with $Na_2S$ treatment, a well with only NTSH treatment, and a well with NTSH and $Na_2S$ treatments were maintained. All experiments were conducted in replicates. After adding 4′,6-diamidino-2-phenylindole (DAPI), three washings were provided within a time gap of 2 min. Later, coverslips were mounted, and a fluorescent microscope was used to observe the emission intensity.

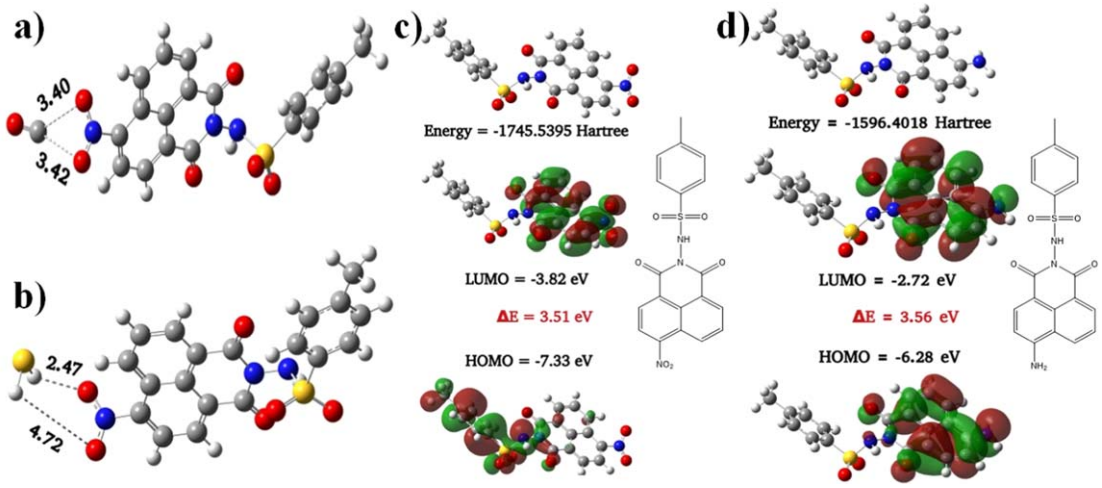


**Figure 1.** (a)) Interactions of NTSH with (a) CO and (b) $H_2S$. HOMO–LUMO energy gaps of (c) NTSH and (d) reduced NTSH.

## 3. Results and discussion

### 3.1. Theoretical studies

After the probe design, the binding affinity of NTSH towards $H_2S$ over CO was explored using theoretical simulations. Binding energy studies are crucial for understanding the interaction of $H_2S$ with the nitro group present in the chemical structure of the designed probe. Hence, the binding affinity of NTSH with both the gasotransmitters CO and $H_2S$, which are good reducing agents, are investigated and compared. It is observed that the electropositive carbon of CO interacts with both oxygen atoms of $NO_2$ as shown in figure 1(a), while both the hydrogens in $H_2S$ bind with the oxygens of $NO_2$ as portrayed in figure 1(b). The calculated energies reveal that CO binds favorably with the $NO_2$ site, with a binding energy of 0.82 kcal $mol^{-1}$. Conversely, $H_2S$ interaction with NTSH exhibits relatively higher stabilization energy of 2.07 kcal $mol^{-1}$. These interaction patterns between NTSH and the two studied gasotransmitters suggest that $H_2S$ has a stronger affinity for $NO_2$ compared to CO. Subsequently, the HOMO and LUMO levels of NTSH and the expected reduction product of NTSH (reduced NTSH: toluene sulphonyl hydrazide attached amino napthalimide) were examined. The initial energy gap value of 3.51 eV for NTSH was found to shift to 3.56 eV in its amino counterpart. This investigation thus highlights the impact of nitro-to-amino conversion on the energy gap, as portrayed in figures 1(c) and (d). The increase in the energy gap when nitro group is replaced with amino functionality due to the expected reduction reaction suggests a potential alteration in the electronic properties of the molecule, which could contribute to the changes in the electronic spectrum of NTSH. The theoretical studies thus offer insightful information about the relationships between molecular structure and electronic and optical characteristics, illustrating its possible applications and behavior as a $H_2S$ sensing probe.

### 3.2. Characterisation of 4-methyl-*N*-(6-nitro-1,3-dioxo-1*H*-benzo[*de*]isoquinolin-2(3*H*)yl) benzenesulfonamide (NTSH)

Based on the results obtained through theoretical calculations, NTSH was prepared by condensing the commercially available 4-nitro-1,8-naphthalic anhydride with *p*-toluene sulphonyl hydrazide in glacial acetic acid at 118 °C. Acetic acid acts as a proton source and a catalyst. It also facilitates the condensation reaction. The proposed mechanism is depicted in scheme 1(b). A successful workup phase was achieved by neutralizing the acid with the measured addition of 10% (w/v) sodium bicarbonate solution to obtain NTSH from its nascent state to its final, purified form. Precise control of temperature and reaction duration, followed by careful neutralization during the workup phase is crucial to obtain pure NTSH. The new naphthalimide derivative was structurally confirmed using spectral techniques. The $^1$H NMR spectrum revealed nine aromatic protons and three methyl protons, while the $^{13}$C NMR indicated the presence of 19 carbons in the NTSH structure. The IR spectrum showed characteristic peaks corresponding to NH stretch, C=C, C=O, and S=O. In the mass spectrum, NTSH exhibited M+1 and M+23 peaks at m/z values of 412.05 and 434, respectively. Since $H_2S$ detection by NTSH relies on the nitro-to-amino group transformation, the mass spectrum of reduced NTSH (toluene sulfonyl hydrazide-conjugated amino naphthalimide) was also recorded, which showed an M+1 peak at m/z = 382.12. The characterization data provided below agrees with the designed structure of NTSH.

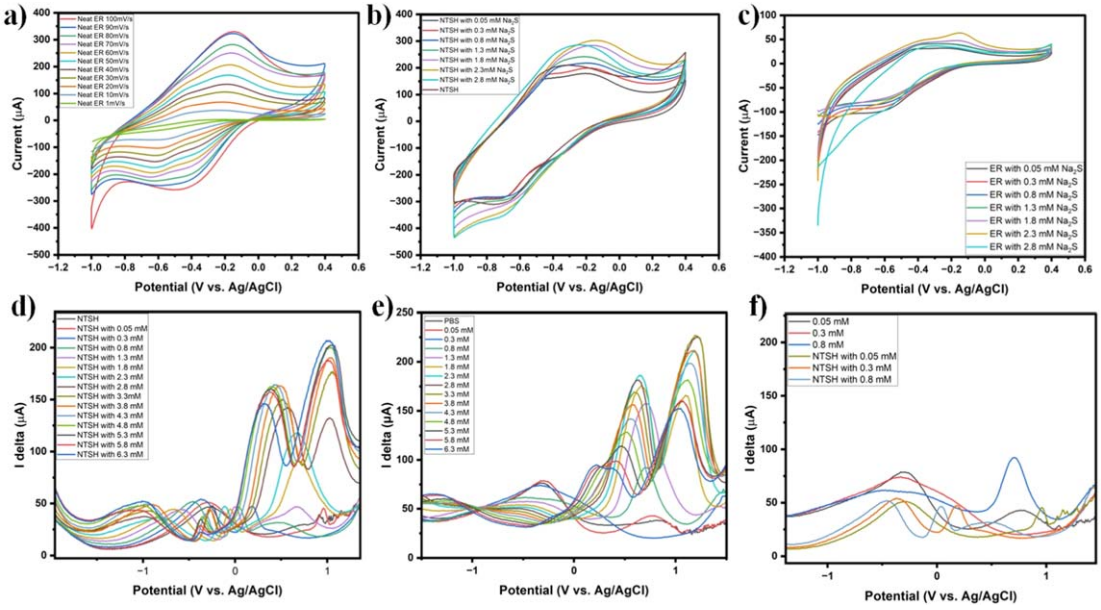


**Figure 2.** Cyclic voltammograms of (a) neat NTSH at different scan rates and NTSH in the presence of $Na_2S$ at (b) 100 and (c) 10 mV $s^{-1}$. square wave voltammograms of (d) NTSH with $Na_2S$ and (e) neat $Na_2S$ (0.05–6.3 mM). (f) Comparison plots of 0.05 and 2.8 mM $Na_2S$, NTSH, and NTSH with 0.05 and 2.8 mM $Na_2S$.

NTSH: 71.23%, 172-174 °C. FTIR ($cm^{-1}$): 785, 1336, 1508, 1682, 1780, 3396 (**Supplementary figure** (**SF**) **1**); $^1$H NMR (400 MHz, ppm): 2.471 (s, $CH_3$, 3H), 7.342–7.360 (d, 7.2 Hz, 2H), 7.875–7.894 (d, 7.6 Hz, 2H), 8.019–8.038 (d, 7.6 Hz, 1H), 8.397–8.416 (d, 7.6 Hz, 1H), 8.694–8.747 (m, 2H), 8.866–8.886 (d, 8 Hz, 1H) (**SF2**); $^{13}$C NMR (100 MHz): 20.75, 121.18, 122.83, 125.09,127.29,127.75,128.67,129.07,129.33,129.42,129.86,130.03,132.59,133.68,134.48,144.09,149.28,159.39, 160.19 (**SF3**); MS (m/z) of $C_{19}H_{13}N_3O_6S$: 412.05 (M+1), 434.04 (M+23) (**SF4a**). MS (m/z) of $C_{19}H_{15}N_3O_4S$ (reduced NTSH): 382.12 (M+1) (**SF4b**).

### 3.3. Electrochemical studies

Cyclic voltammograms of neat NTSH (100 μM) were recorded to examine its response across different scan rates without adding $Na_2S$ (figure 2(a)). Increase in concentration of $Na_2S$ with NTSH (100 μM) at 100 mV $s^{-1}$ (figure 2(b)), and 10 mV $s^{-1}$ (figure 2(c)) were studied in the potentials sweep window of −1.2–0.6 V versus Ag/AgCl. In figure 2(a), peak currents (Ipa and Ipc) showed a rise with an increase in the scan rate, indicating adsorption-controlled kinetics for the system as depicted in **SF5**. Additionally, anodic peak (−0.18 V) can be observed in the positive potential direction, which might be due to the oxidation of the hydroxylamine derivative (R-NH-OH) to generate the nitroso derivative (R-N = O). During the reverse scan, the reduction of the nitroso derivative becomes evident at the cathodic peak of −0.4 V. These two peaks form a quasi-reversible couple [29] as described by the following equation [30]:

$$R - NH - OH \leftrightharpoons R - N = O + 2e^- + 2H^+$$

A 0.2 V shift in the forward and backward scan was observed in figure 2(b) compared to the CV of figure 2(a) for neat NTSH. Although the reagents are the same, stirring conditions were provided for figure 2(b) as it involves the addition of $Na_2S$ at different intervals. The stirring brought about changes in migration, convection, and diffusion of ions in the system. However, the overall electrochemical behavior remains consistent, and the shift does not affect the key conclusions of the study. As the $Na_2S$ concentration increases (figure 2(b)), the anodic peak at −0.16 V region becomes predominant due to oxidation of $Na_2S$. This behavior can be expected due to the thermodynamic oxidation potentials of $H_2S$. The oxidation of $H_2S$ at lower potentials leads to the formation of insoluble elemental sulphur [31, 32].

$$H_2S \rightarrow S + 2H^+ + 2e^-;\ E_0 = -0.14V$$

$$SO_2 \rightarrow S + O_2;\ E_0 = 0.17V$$

Moreover, as the $Na_2S$ concentration increases, the quasi-reversible couple may disappear, and nitro reduction to amine may commence. Therefore, the oxidation peak observed at higher concentrations of $Na_2S$ in the forward scan might be due to sulfur oxidation, while the cathodic peak could be attributed to nitro reduction. The same trend is observed at the scan rate of 10 mV $s^{-1}$ (figure 2(c)), with only a difference in sharper

peaks than the CV pattern of 100 mV $s^{-1}$. However, the reduction potentials of nitroarenes in NTSH may be influenced by various factors such as solvent, pH, electrode, and substituents on the aryl ring [33–36].

SWVs were measured: increase in $Na_2S$ with NTSH (figure 2(d)), increase in $Na_2S$ without NTSH (figure 2(e)), and comparison between them (figure 2(f)) in the potential range of −2 V to 2 V, specifically to observe the sulfur oxidation peaks. In figure 2(d), neat NTSH has a single peak at −0.29 V with a current of 46.26 μA. Upon adding 0.05 mM of $Na_2S$, a slight increase in current to 50.75 μA is noted. Further, as the $Na_2S$ concentration increases from 0.05 to 2.3 mM, a new peak emerges at 0.16 V. Finally, for the maximum concentration of $Na_2S$ studied, two peaks are observed at 0.4 and 1 V. As the concentration increased, the peak at −0.29 V for neat NTSH was found to shift negatively towards −0.9 V, possibly due to the reduction of the nitro group. Whereas the peak observed at 0.16 V for 0.05 mM of $Na_2S$ is seen to shift towards the positive window, which might be due to the oxidation of $H_2S$ at the working electrode, which involves the transfer of two electrons ($H_2S \rightarrow S + 2H^+ + 2e^-$), resulting in the current generation [8]. Further oxidation can lead to the formation of sulfite ($SO_3^{2-}$) and sulfate ($SO_4^{2-}$) ions. Therefore, the peaks observed in the positive window with increasing $Na_2S$ concentration can be attributed to sulfur and its oxides, such as $SO_3^{2-}$ and $SO_4^{2-}$. Meanwhile, the shift observed in the negative window can be attributed to changes in the reaction environment as the reduction of the nitro group occurs to amino group. In addition, the current decreased for the peak at the negative window as the $Na_2S$ concentration increased, while the current showed an evident increase in the positive window. This result supports the nitro reduction and sulfur oxidation when the $Na_2S$ concentration increases to a maximum, leading to the complete conversion of the nitro group. Later, sulfur concentration increases in the reaction media, leading to more sulfur oxidation and, thereby resulting in higher current at positive potential. In figure 2(e), SWVs were measured for $Na_2S$ in PBS without the addition of NTSH in which the least concentration, i.e., 0.05 mM, showed two peaks at −0.28 and +0.78 V. As the concentration increases to 6.3 mM, the peak at the negative window is seen to completely disappear, and the two peaks at 0.68 and 1.2 V are found to increase. This might be due to the conversion of adsorbed sulfur into $SO_4^{2-}$ ions. The comparison plots are depicted in figure 2(f) for higher and lower concentrations of $Na_2S$ in PBS with and without NTSH. The neat NTSH has a peak at ∼ −0.3 V and $Na_2S$ has peaks at ∼ 0.6 V and 1.2 V.

Jackson *et al* reported that CVs of $H_2S$ recorded using platinum electrodes displayed three characteristic potentials at −0.1, +0.475, and +1.0 V versus AglAgCl. These features are ascribed to the oxidation of sulfide, the adsorption of elemental sulfur with associated secondary reactions, and the conversion of deposited sulfur into water-soluble $SO_4^{2-}$, respectively [37]. While comparing the square wave voltammograms of neat $Na_2S$ and NTSH with $Na_2S$, important observations analogous to reports by Jackson *et al* are perceived in the present study. Oxidation of sulfide occurs at −0.1 V for blank $Na_2S$ at lower concentrations. For higher concentrations, direct sulfur deposition occurs at 0.4 V. Oxidation of sulfide is retained at −0.1 V by NTSH, as in the case of lower $Na_2S$ concentration. Moreover, the adsorption of elemental sulfur is shifted to a higher potential of 0.6 V, which indicates that NTSH maintains oxidation of elemental sulfur as the nitro group consumes the electrons to get reduced to the amino group. Hence, the sulfur deposition does not happen below 0.6 V. However, deposited sulfur dissolves back as sulfates at 1V [37]. The XPS spectra were recorded after electrochemical measurements to confirm the presence of sulfates, sulfites, and elemental sulfur. The survey scan spectra and full scan spectra are presented in **SF6a** and **SF6b**. It showed peaks at 163.03 eV, 168.9 eV, and 167.4 eV for elemental sulfur, sulfates, and sulfites, respectively [38].

Moreover, thin-layer chromatography (TLC) was performed after every CV measurement performed as in figure 2(d). Interestingly, the faint fluorescent blue spot observed under 365 nm UV light illumination for pure NTSH transformed into a green fluorescence spot as the concentration of $Na_2S$ increased, as illustrated in **SF7a** and **SF7b** with a small change in retention factor. Nevertheless, the TLC performed after every CV measurement presented in figure 2(e) did not display any fluorescent green spots under UV light (**SF7c** and **SF7d**). This indicates that the presence of NTSH and the reduction of the nitro group to an amino group are essential for the appearance of green spots. Furthermore, to calculate the LOD ($3\sigma/S$ method), the SWVs were conducted in a lower concentration range of $Na_2S$ (36–50 nM). The LOD was found to be 29 nM with an $R^2$ value of 0.9801, and the limit of quantification (LOQ; $10\sigma/S$ method) was 88.2 nM (**SF8a** and **SF78b**), where $\sigma$ is the standard deviation = standard error $\times \sqrt{n}$; n = 4 and S is the slope of the measurement curve.

### 3.4. Absorbance studies

Absorbance studies of probe NTSH in 1:6 DMSO:PBS were conducted by raising the $Na_2S$ concentration in succession from 0.32–30.2 mM. The maximum absorption wavelength of the probe NTSH was about 352 nm. With the increase in the concentration of $Na_2S$, the absorbance at 352 nm gradually reduced, and a new absorbance peak emerged at 430 nm with a gradual increase in intensity and an isosbestic point at 400 nm, as shown in figure 3(a). This might be due to the formation of $H_2S$-catalyzed reduction of NTSH to its amino

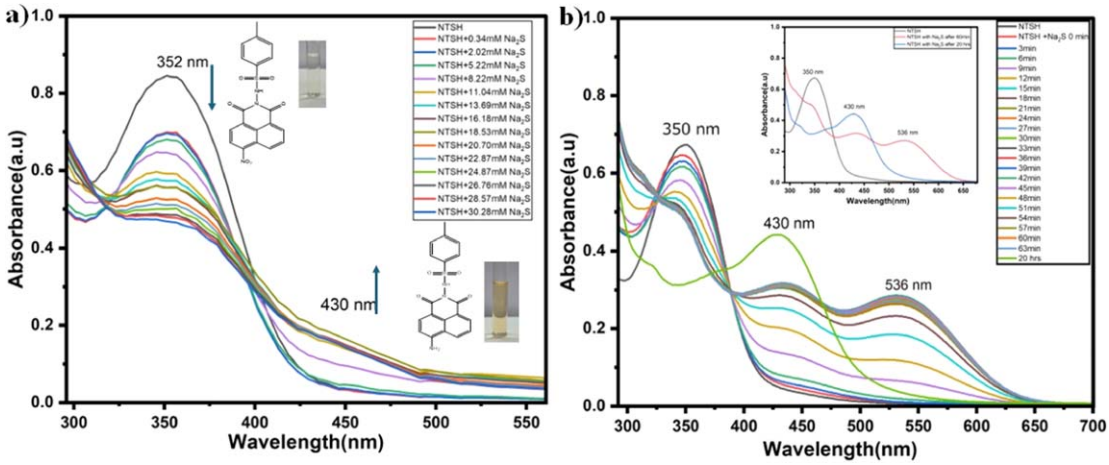


**Figure 3.** (a)) Concentration and (b) time-dependent UV–vis spectra of 100 μM NTSH with $Na_2S$.

counterpart. The LOD of NTSH from UV measurements at ambient temperature is 15.08 mM with an $R^2$ value of 0.923, and LOQ was 45.71 mM (**SF9**).

Further, to closely monitor the reactions, time-dependent variations in the absorbance of NTSH were measured every 3 min. The evident changes within the time frame are portrayed in figure 3(b), which suggests dynamic reactions during the process. A significant finding from the time-dependent study is the appearance of a secondary peak at 536 nm and the absorbance at 430 nm. This peak could be attributed to the formation of an intermediate during the initial phases of the reaction. This absorption peak disappeared in the spectrum recorded after 20 h of $Na_2S$ addition (figure 3(b)), suggesting the transient nature of the intermediate and confirming the completion reaction to observe a single absorbance peak at 430 nm. The inset image (figure 3(b)) compares the absorption due to electronic transitions in NTSH as well as those after 1h and 20 h of $Na_2S$ treatments. During the absorbance studies, the transformation of the colorless reaction mixture into light brown after 20 h of $Na_2S$ addition inspired us to conduct colorimetric studies.

### 3.5. Colorimetric studies

To check the colorimetric sensing efficacy of NTSH, absorbance at 430 nm was recorded for the product formed after each incremental concentration of $Na_2S$. The transformation from colorless to light brown could be linked to the interaction between $Na_2S$ and NTSH, potentially involving converting the nitro group attached to the naphthalimide unit to the amino group. The color changes cannot be attributed to the protonation of the tosylate group present on the NTSH because $Na_2S$ in PBS maintains the pH around neutral, and the tosylates need acidic conditions to get protonated. The LOD of NTSH from colorimetric measurements is found to be 2.48 mM with an $R^2$ value of 0.999 and LOQ of 7.52 mM from the calibration curve (**SF10**).

### 3.6. Emission studies

Subsequently, the ability of NTSH to serve as an $H_2S$-responsive fluorescent probe was explored. The 3D emission spectrum recorded for NTSH displayed maximum excitation at 430 nm (figure 4(a)) and weak emission at 550 nm. The free probe showed weak fluorescence due to the photoinduced electron transfer mechanism (PET) resulting from the electron pull of the nitro group [27]. However, with $Na_2S$ addition, a significant fluorescence turn-on response at 550 nm was observed ($\lambda_{ex} = 430$ nm). The emission of NTSH exhibited significant changes in the fluorescence intensity upon a gradual increase in $Na_2S$ concentrations. A large enhancement in fluorescence intensity was observed upon the addition of 26.76 mM $Na_2S$, as presented in figure 4(b). The variations in the emission features were perceptible to the human eye as a transition in fluorescence color from blue to yellowish green under 365 nm UV illumination, while it shifted from colorless to light brown when examined under daylight (**SF11**). Later, the concentration and time-dependent emission features of NTSH were studied for lower concentrations (250–1000 μM) of $Na_2S$ and the earliest measurement having a time gap of 5 s after adding $Na_2S$ (**SF12** and figure 4(c)). The changes in the emission intensity observed with high $Na_2S$ concentrations are depicted in the bar chart (figure 4(d)). The fluorescence intensity of the probe exhibited growth in correlation with both time and concentration, indicating a shift away from the PET mechanism and towards intramolecular charge transfer (ICT) [39], serving as an indication of the $H_2S$-induced reduction of the nitro group to amino chromophore. The emission studies thus revealed the prospective use of

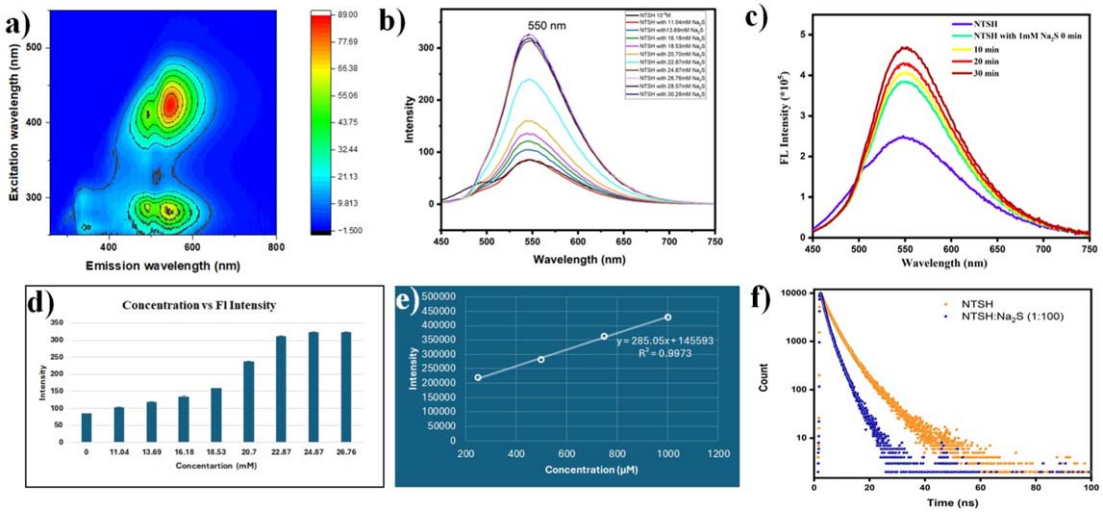


**Figure 4.** (a) 3D spectrum of NTSH. (b) 2D emission spectra of NTSH in presence of $Na_2S$ of 11.04–26.76 mM; $\lambda_{ex} = 430$ nm. (c) Time-dependent emission spectra of NTSH in the presence of 1 mM $Na_2S$. (d) Bar diagram representing concentration versus fluorescence intensity of NTSH in the presence of $Na_2S$ of 11.04–26.76 mM, (e) Calibration curve for determination of LOD, and (f) time-dependent fluorescence lifetime decay spectra of NTSH and NTSH with $Na_2S$.

NTSH as a turn-on fluorescent probe. The LOD of NTSH from fluorescence measurements is 166 μM with an $R^2$ value of 0.997 and LOQ of 504.08 μM (figure 4(e)).

The fluorescence lifetime studies provide information about the time a fluorophore takes for transition from an excited state to the ground state, following the absorption of a photon and subsequent fluorescence emission. The lifetime measurements [40] of pure NTSH and in the presence of 1 mM $Na_2S$ were investigated and represented pictorially in figure 4(f). The related parameters of fluorescent lifetimes of NTSH and NTSH with $Na_2S$ are listed in Supplementary table (ST) 1. The average lifetimes ($\tau_1$ and $\tau_2$) of the excited states of the NTSH in the absence of $Na_2S$ are found to be 2.68 and 6.27 ns, respectively. However, upon adding $Na_2S$, the lifetime values drastically changed to 1.55 and 3.71 ns, respectively, confirming $Na_2S$ triggered reaction and subsequent product formation. The observed decrease in fluorescence lifetimes could be attributed to the interaction of $H_2S$ with the nitro group present on NTSH, leading to changes in the electronic structure and environment of the fluorophore (conversion of nitro to amino group). This alteration may result in faster decay of the excited state and, hence, shorter fluorescence lifetimes. These lifetime values could suggest the presence of different conformations, environments, or interaction dynamics of NTSH molecules, leading to different rates of fluorescence emission decay.

### 3.7. Fluorescence imaging of HEK293T cells

Initially, the selectivity of NTSH for $H_2S$ compared to other sulfur-containing biological reducing agents, like Cys and GSH, was investigated. It is observed from **SF13** that NTSH showed comparatively higher fluorescence intensity compared with other sulfur-containing analytes. Further, to check the biocompatibility of NTSH, a cell viability assay was performed in HEK293T cells. The cells were treated with different concentrations of NTSH, ranging from 5 to 30 μM. The MTT results showed that cell viability was concentration-dependent, with 90% viability at 5 μM concentration (**SF14**). However, a decrease in cell viability was observed with an increase in fluorophore concentration. A concentration of 5 μM of NTSH was chosen to perform further experimental assessments, giving the best possible balance between fluorophore concentration and cell survival.

The sulfomic index measures the S-oxide redox status, providing a profile of endogenous sulfur in various oxidation states. Scrivner *et al* have measured the levels of endogenous $H_2S$ alongside small sulfur oxoacids (SOS = HOSH, HOSOH) in various cell lines, including HEK293T cells [41]. They found that both $H_2S$ and its S-oxide derivatives exhibit continuous extrusion into the surrounding media against a concentration gradient, indicating an active efflux process in these cells. Inhibition of several enzymes responsible for $H_2S$ generation by small molecules suggests that SOS are not exclusively derived from $H_2S$ oxidation. Even after successfully inhibiting $H_2S$ production, cells maintain a steady efflux and replenish $H_2S$ and SOS over time. This research demonstrates that these small sulfur oxoacids are synthesized in cells of diverse types, and their efflux suggests a role in cellular signaling and potentially other vascular physiological processes associated with $H_2S$. Our study included (i) control wells containing untreated cells and treated cells: (ii) only with $Na_2S$, (iii) only with NTSH, and (iv) together with NTSH and $Na_2S$ to maintain accuracy and avoid bias. The imaging was done in both green

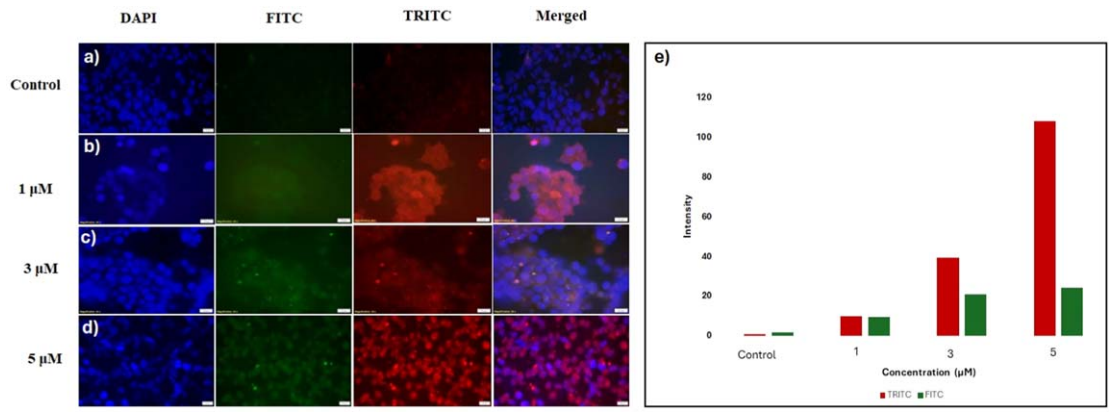


**Figure 5.** Cell images using (a) control, and (b) 1μM, (c) 3 μM and (d) 5 μM of NTSH (e) Comparison of concentration (NTSH) dependent fluorescence intensity between FITC and TRITC filters.

Fluorescein isothiocyanate (FITC) and red Tetramethylrhodamine isothiocyanate (TRITC) filters, and it was found that the green filter showed less fluorescence when compared to red, as presented in figures 5(a)–(d). The observed phenomenon where the red filter images displayed higher fluorescence compared to the green filter correlates well with the emission wavelength of NTSH at 550 nm. It is an added benefit to have stronger emission in the red filter, as it removes the possibility of autofluorescence, improves the signal-to-background ratio, and enhances the specificity of the fluorescence signal from the NTSH.

Furthermore, the cells were treated with different concentrations of NTSH (1–5 μM); the acquired images are presented in figures 5(a)–(d). Interestingly, the probe is successful even in imaging HEK293T cells that contain only NTSH without adding external $Na_2S$ under $< 30$ min incubation time. This might be due to the successful sensing of endogenous $H_2S$ present in the HEK293T cells by NTSH, as reported by Scrivner *et al* [41]. In other words, the conversion of the nitro group happens inside the cells due to the endogenous $H_2S$ present. The bar chart, as portrayed in figure 5(e), compares the fluorescence intensity from FITC and TRITC filters of control cells and cells treated with different concentrations of NTSH; the data indicates that the emission wavelength of the probe aligns with the red filter, suggesting that the probe is better suited for use with the red filter for cell imaging.

Furthermore, the cells were treated with 5 μM NTSH, and imaging experiments were performed in HEK293T cells with and without the addition of $Na_2S$. It is observed that in the presence of externally supplied $Na_2S$, the cells were highly fluorescent. This could be because of the availability of higher $H_2S$ concentration inside the cell and a greater number of nitro groups getting converted to amino groups, whereas this phenomenon is absent in the control figures 6(a)–(d). The bar chart in figure 6(e) compares the fluorescence intensity levels of control cells, cells treated only with $Na_2S$, and cells treated with NTSH, both with and without externally supplied $Na_2S$. The intensity increased by 3.5-fold in cells treated with external $Na_2S$ (figure 6(c)) compared to those treated with NTSH alone figure 6(d). This demonstrates that the cells respond to both exogenous and endogenous $Na_2S$ in the presence of NTSH, indicating that NTSH is an effective probe for sensing intracellular $H_2S$. The study thus reveals the successful development of a fluorescence probe, NTSH, capable of sensing $H_2S$ in cellular environments, leveraging its chemical transformation in the presence of $H_2S$. The probe's efficacy in detecting endogenous $H_2S$ within HEK293T cells was confirmed through meticulous experimental design and imaging techniques. The increased fluorescence intensity observed upon adding exogenous $Na_2S$ further underscores the probe's sensitivity to $H_2S$ levels.

Notably, a few reported naphthalimide probes utilize the reduction of nitro to amino group for $H_2S$ sensing. Angela Bamesberger *et al* reported a fluorescent probe where nitro napthalimide is attached with o-phenylenediamine that exhibited a linear relationship with $H_2S$ concentrations ranging from 0 to 100 μM, which aligns with the typical $H_2S$ levels found in biological systems. They mentioned the range of linearity for $H_2S$ response, but the detection limit of the probe was not specified [27]. Naha *et al* reported a probe synthesized from 3-nitro-1,8-napthalic anhydride and formic hydrazide, which solely exhibited a colorimetric response to $H_2S$. The researchers reported a chemo-dosimetric reduction of the nitro group in the presence of $H_2S$, with a LOD of 8.1 μM [42]. The study by Ranjith and coworkers reported a N-aryl-1,8-naphthalimide-based probe that showed a dual-emission and dual-channel optical response for detecting sulfide in aqueous solution. This $H_2S$ detection system incorporates both azido and nitro functional groups as $H_2S$ sensing sites on a single fluorescent platform with a detection limit between 0.1 and 0.5 μM [43]. Montoya and his team created a probe by reacting 4-nitro-1,8-napthalimide with 2-methoxyethyl amine in ethanol, which showed a 15-fold turn-on fluorescence

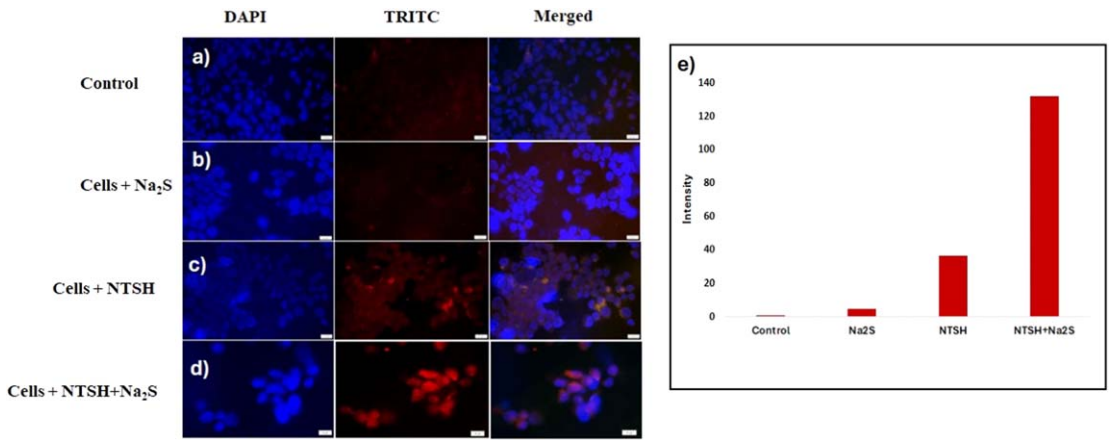


**Figure 6.** Cell images (a) Control (b) only $Na_2S$, (c) 5 μM NTSH, and (d) NTSH with $Na_2S$. (e) Comparison of fluorescence intensity from cells treated with $Na_2S$, NTSH, and a combination of $Na_2S$ and NTSH using TRITC filter.

after 90 min, and LOD of 5–10 μM [23]. Though the $H_2S$ detection limits of NTSH using absorbance and colorimetric methods are higher than some reported sensors, the probe still provides robust options in the application front. The response of NTSH to $H_2S$ detectable through colorimetric, fluorometric and electrochemical approaches enhances its practicality and adaptability in various environments, a feature that many of the other probes do not offer. Most of the probes are limited to fluorescence or colorimetry, which can restrict their application scope.

## 4. Conclusion

A new nitronaphthalimide derivative NTSH synthesized by easy imidation reaction showed versatile applicability as a $H_2S$ sensor with detection limits of 166 μM in fluorometric, 15.08 mM in absorbance, 2.48 mM in colorimetric, and 29 nM in electrochemical methods. The fluorescent probe NTSH, incorporating a 1,8-naphthalimide fluorescent platform and a nitro group responsive site, significantly increases fluorescent emission at 550 nm upon adding $Na_2S$. By combining electrochemical detection with colorimetric and fluorometric methods, NTSH sets a new standard for multifunctional probes, potentially paving the way for future research and applications in developing naphthalimide-based sensors. This study could stimulate further exploration of electrochemical methods for other naphthalimide derivatives, expanding the toolkit available for $H_2S$ sensing and beyond. Significantly, NTSH has demonstrated effectiveness in bioimaging applications, particularly in detecting endogenous $H_2S$ in HEK 293T cells, underscoring its utility in chemical biology research. The successful synthesis and multifaceted application of NTSH aligns with the ongoing scientific focus on developing advanced probes for various analytical and imaging purposes. Future studies could investigate the potential of the probe for organelle-specific detection of $H_2S$, particularly in the endoplasmic reticulum (ER), thereby expanding its applicability in cellular and biomedical research.

## Data availability statement

The data cannot be made publicly available upon publication because they are not available in a format that is sufficiently accessible or reusable by other researchers. The data that support the findings of this study are available upon reasonable request from the authors.

## Funding

This research received no specific grant from any funding agency in the public, commercial, or not-for-profit sectors.

## Data availability

Supplementary data is provided. The datasets generated during and/or analyzed during the study are available from the first author on reasonable request.

## Conflicts of interest

There are no conflicts to declare.

## ORCID iDs

Dhanya Sunil https://orcid.org/0000-0002-0727-5125
Sudhakar Y N https://orcid.org/0000-0001-5051-4438
Sivaranjana Reddy Vennapusa https://orcid.org/0000-0002-8252-9586

## References

[1] Chen C J, Cheng M C, Hsu C N and Tain Y L 2023 Sulfur-containing amino acids, hydrogen sulfide, and sulfur compounds on kidney health and disease *Metabolites* **13** 688
[2] Yang Y L, Zhang K, Zhou Z T, Jiang Z L, Liu Y, Zhang Y X, Liu Z H, Ji X Y and Wu D D 2022 The role of hydrogen sulfide in the development and progression of lung cancer *Molecules* **27** 9005
[3] Li X *et al* 2022 Hydrogen sulfide and its donors: keys to unlock the chains of nonalcoholic fatty liver disease *Int. J. Mol. Sci.* **23** 12202
[4] Módis K, Wolanska K and Vozdek R 2013 Hydrogen sulfide in cell signaling, signal transduction, cellular bioenergetics and physiology in *C. elegans General Physiology and Biophysics,* **32** 1–22
[5] Szabó C 2007 Hydrogen sulfide and its therapeutic potential *Nat Rev Drug Discov* **6** 917–35
[6] Szabo C, Ransy C, Módis K, Andriamihaja M, Murghes B, Coletta C, Olah G, Yanagi K and Bouillaud F 2014 Regulation of mitochondrial bioenergetic function by hydrogen sulfide. Part I. biochemical and physiological mechanisms *Br. J. Pharmacol.* **171** 2099–122
[7] Filipovic M R, Zivanovic J, Alvarez B and Banerjee R 2018 Chemical biology of $H_2S$ signaling through persulfidation *Chem. Rev.* **118** 1253–337
[8] Cao X, Ding L, Xie Z, Yang Y, Whiteman M, Moore P K and Bian J-S 2019 A review of hydrogen sulfide synthesis, metabolism, and measurement: is modulation of hydrogen sulfide a novel therapeutic for cancer? *Antioxid. Redox Signal.* **31** 1–38
[9] Feng X, Chen Y, Zhao J, Tang C, Jiang Z and Geng B 2009 Hydrogen sulfide from adipose tissue is a novel insulin resistance regulator *Biochem. Biophys. Res. Commun.* **380** 153–9
[10] Li H *et al* 2020 Small-molecule fluorescent probes for $H_2S$ detection: advances and perspectives *Trends in Analytical Chemistry* **116** 117
[11] Xu T, Scafa N, Xu L-P, Zhou S, Al-Ghanem K A, Mahboob S, Fugetsu B and Zhang X 2016 Electrochemical hydrogen sulfide biosensors *Analyst* **141** 1185–95
[12] Levitt M D, Abdel-Rehim M S and Furne J 2011 Free and acid-labile hydrogen sulfide concentrations in mouse tissues: anomalously high free hydrogen sulfide in aortic tissue *Antioxid Redox Signal* **15** 373–8
[13] Yang L, Zhao J, Yu X, Zhang R, Han G, Liu R, Liu Z, Zhao T, Han M-Y and Zhang Z 2018 Dynamic mapping of spontaneously produced $H_2S$ in the entire cell space and in live animals using a rationally designed molecular switch *Analyst* **143** 1881–9
[14] Yang L, Niu J Y, Sun R, Xu Y-J and Ge J-F 2018 Rosamine with pyronine-pyridinium skeleton: unique mitochondrial targetable structure for fluorescent probes *Analyst* **143** 1813–9
[15] Zhao Q, Yin C, Kang J, Wen Y and Huo F 2018 A viscosity sensitive azide-pyridine BODIPY-based fluorescent dye for imaging of hydrogen sulfide in living cells *Dyes Pigm.* **159** 166–72
[16] Liu J, Chen X, Zhang Y, Gao G, Zhang X, Hou S and Hou Y 2018 A novel 3-hydroxy chromone fluorescent probe for hydrogen sulfide based on an excited-state intramolecular proton transfer mechanism *New J. Chem.* **42** 12918–23
[17] Zhang W, Jia Q, Meng Y, Chen S, Zhang Y, Wang K-P, Gan L-H and Hu Z-Q 2020 Dimethylamino naphthalene-based fluorescent probes for hydrogen sulfide detection and living cell imaging *Spectrochim. Acta A Mol. Biomol. Spectrosc.* **228** 117835
[18] Peng S, Wang Y, Wang X, Ma Y and Zhang X 2018 A novel fluorescent probe for selective detection of hydrogen sulfide in living cells *New J. Chem.* **42** 5185–92
[19] Jun Y W, Kim H R, Reo Y J, Dai M and Ahn K H 2017 Addressing the autofluorescence issue in deep tissue imaging by two-photon microscopy: the significance of far-red emitting dyes *Chem. Sci.* **8** 7696–704
[20] Zhang Y, Tang Y, Kong X and Lin W 2021 An endoplasmic reticulum targetable turn-on fluorescence probe for imaging application of carbon monoxide in living cells *Spectrochim Acta A Mol Biomol Spectrosc* **247** 119150
[21] Dhara K, Lohar S, Patra A, Roy P, Saha S K, Sadhukhan G C and Chattopadhyay P 2018 A new lysosome-targetable turn-on fluorogenic probe for carbon monoxide imaging in living cells *Anal. Chem.* **90** 2933–8
[22] Sarkar A, Fouzder C, Chakraborty S, Ahmmed E, Kundu R, Dam S, Chattopadhyay P and Dhara K 2020 A nuclear-localized naphthalimide-based fluorescent light-up probe for selective detection of carbon monoxide in living cells *Chem. Res. Toxicol.* **33** 651–6
[23] Montoya L A and Pluth M D 2012 Selective turn-on fluorescent probes for imaging hydrogen sulfide in living cells *Chem. Commun.* **48** 4767–9
[24] Tang Y, Ma Y, Xu A, Xu G and Lin W 2017 A turn-on fluorescent probe for endogenous formaldehyde in the endoplasmic reticulum of living cells *Methods. Appl. Fluoresc.* **5** 024005
[25] Tang Y, Xu A, Ma Y, Xu G, Gao S and Lin W 2017 A turn-on endoplasmic reticulum-targeted two-photon fluorescent probe for hydrogen sulfide and bio-imaging applications in living cells, tissues, and zebrafish *Sci Rep.* **7** 12944
[26] Xu A, Tang Y and Lin W 2018 Endoplasmic reticulum-targeted two-photon turn-on fluorescent probe for nitroreductase in tumor cells and tissues *Spectrochim Acta A Mol Biomol Spectrosc* **204** 770–6
[27] Bamesberger A, Kim G, Woo J and Cao H 2015 Reduction of nitro group on derivative of 1,8-napthalimide for quantitative detection of hydrogen sulfide *Journal of Fluorescence* **25** 25–9
[28] Hawes C S, Byrne K, Schmitt W and Gunnlaugsson T 2016 Flexible porous coordination polymers from divergent photoluminescent 4-oxo-1,8-naphthalimide ligands *Inorg. Chem.* **55** 11570–82
[29] Squella J, Bollo S and Nunez-Vergara L 2005 Recent developments in the electrochemistry of some nitro compounds of biological significance *Curr. Org. Chem.* **9** 565–81
[30] Grimshaw J 2000 *Electrochemical Reactions and Mechanisms in Organic Chemistry* (Elsevier)
[31] Cross P F 2013 Sulphur dioxide conversion to elemental sulphur by reduction with hydrocarbon fuels *U.S. Patent* 1213760

[32] Nougayrede J 2000 Method for eliminating $H_2S$, $SO_2$, COS and/or $CS_2$ sulfur compounds, contained in a sulfur factory waste gas with recuperation of said compounds in the form of sulfur *EA Patent* 199900048A
[33] Kolluru G K, Shen X and Kevil C G 2013 A tale of two gases: NO and $H_2S$, foes or friends for life? *Redox Biol* **1** 313–8
[34] Eckert W 1998 Electrochemical identification of the hydrogen sulfide system using a $pH_2S$ (glass/Ag°, $Ag_2S$) electrode *J. Electrochem. Soc.* **145** 77–9
[35] Vijayalakshamma S K and Subrahmanya R S 1969 Studies of the polarographic and coulometric behaviour of aromatic nitro-compounds: I. Nitrobenzene in ethanol *J. Electroanal. Chem. Interfacial Electrochem.* **23** 99–114
[36] Wirtanen T, Rodrigo E and Waldvogel S R 2020 Recent advances in the electrochemical reduction of substrates involving N−O bonds *Adv. Synth. Catal.* **362** 2088–101
[37] Hall J R and Schoenfisch M H 2018 Direct electrochemical sensing of hydrogen sulfide without sulfur poisoning *Anal. Chem.* **90** 5194–200
[38] Fantauzzi S F M, Elsener B, Atzei D, Rigoldi A and Rossi A 2015 Exploiting XPS for the identification of sulfides and polysulfides *RSC Adv.* **5** 75953–61
[39] Duke R M, Veale E B, Pfeffer F M, Kruger P E and Gunnlaugsson T 2010 Colorimetric and fluorescent anion sensors: an overview of recent developments in the use of 1,8-naphthalimide-based chemosensors *Chem. Soc. Rev.* **39** 3936–53
[40] Xie L, Fan T, Yao R, Mu Y, Wang R, Fan C and Pu S 2023 Highly selective near-infrared fluorescent probe with large Stokes shift and sensitivity for H2S detection in water, foodstuff and imaging in living cells *Dyes Pigments* **208** 110828
[41] Scrivner O, Kumar M R, Sorokolet K, Wong A, Kebaara B and Farmer P J 2021 Characterization of endogenous and extruded $H_2S$ and small oxoacids of sulfur (SOS) in cell cultures *ACS Chem. Biol.* **16** 1413–24
[42] Naha S, Wu S-P and Velmathi S 2020 Naphthalimide based smart sensor for $CN^-/Fe^{3+}$ and $H_2S$. Synthesis and application in RAW264.7 cells and zebrafish imaging *RSC Adv.* **10** 8751–9
[43] Meka R K and Heagy M D 2017 Selective modulation of internal charge transfer and photoinduced electron transfer processes in N-Aryl-1,8-naphthalimide derivatives: applications in reaction-based fluorogenic sensing of sulfide *J. Org. Chem.* **82** 12153–61